Longitudinal and transverse diffusion of conduction-electron spins on stacks of fluoranthene radical cations

David Saez de Jauregui
Physikalisches Institut, Universität Karlsruhe (TH), D-76128 Karlsruhe, Germany

Jürgen Gmeiner
Bayreuther Institut für Makromolekülforschung, Universität Bayreuth, D-95440 Bayreuth, Germany

Elmar Dormann
Physikalisches Institut, Universität Karlsruhe (TH), D-76128 Karlsruhe, Germany

(Received 13 September 2006; published 6 December 2006)

The temperature dependence and anisotropy of the conduction-electron spin diffusion coefficient $D(T)$ of three single crystals of the organic conductor $(\text{fluoranthene})_2PF_6$ with defect content varying between 7×10^{-5} and 1% per formula unit have been determined. $D_\parallel/D_\perp$ varies between 2×10^4 and 100 in the metallic phase. The defect dependences of the Peierls transition, microwave conductivity, magnetic susceptibility, and transverse relaxation rate are presented as well and their relations are discussed.

DOI: 10.1103/PhysRevB.74.235104 PACS number(s): 71.30.+h, 71.45.Lr, 72.15.Lh, 76.30.Pk

I. INTRODUCTION

There is a continuing debate whether real low-dimensional conductors, tending to a charge-density-wave (CDW) ground state, can be described within the Luttinger liquid model, and whether their electrical conductivity follows a power law or thermally activated behavior.[1–4] On the other hand, solitonlike descriptions of the lowest-energy spin and charge carriers were introduced for the kinks of the dimerization sequence.[5–10] Unfortunately, the prototype examples of inorganic Peierls systems like $NbSe_3$ are not really one dimensional in their conduction band structure and the sample preparation techniques required to produce the quasi-one-dimensional behavior may be suspected of producing uncontrolled defects as well.

In order to provide a reliable characterization of an "ideal" quasi-one-dimensional (1D) conductor with signatures of CDW fluctuations in the metallic high-temperature phase and x-ray-demonstrated three-dimensionally (3D) ordered Peierls distorted low-temperature phase,[11,12] we establish in this paper the anisotropy, temperature, and defect dependence of the diffusion coefficients $D_\parallel$ and $D_\perp$ of the conduction-electron spins in difluoranthene phosphorus hexafluoride $(FA)_2PF_6$ $(FA=C_{16}H_{10})$. This is the best-defined one-dimensional conductor of the family of radical cation salts that can be grown by electrochemical techniques from one of the arenes naphthalene, fluoranthene, pyrene, or perylene and PF_6, AsF_6, or SbF_6 as inorganic anions.[13–15] The crystal structure shows $(FA)_2^{+\cdot}$ dimers stacked along the crystallographic a direction, with neighboring FA molecules rotated by 180°.[14–16] Above the Peierls transition ($T_P\approx180-186$ K) a structural phase transition is observed at about $T_S\approx202$ K, with doubling of the perpendicular-to-stack periodicity by counterrotation of the neighboring FA stacks and reduction of the space group symmetry from $A2/m$ to $P2_1/c$.[15–18] Occasionally, single crystals show growth sectors, with varying concentration of localized defects. Furthermore, the formation of twins has been observed, with 180° rotation around the stacking axis a as the twinning law.[19] Care was taken to avoid such complication in the current analysis.

Optical reflectivity, microwave, and direct-current conductivity of $(FA)_2PF_6$ have been measured, and a pronounced anisotropy of charge transport of $\sigma_\parallel/\sigma_\perp=10^4:1$ is established.[17,20–24] Figure 1 shows examples for the microwave conductivity of typical crystals. The unique property of these arene salts is their extremely narrow conduction-electron spin resonance (ESR) line, or correspondingly their extremely long transverse as well as spin lattice relaxation times of the order of 5–10 μs.[25] This is a consequence of the conduction electrons' weak spin-orbit coupling and their highly one-dimensional motion. Figure 2 shows the temperature dependence of the ESR-derived paramagnetic susceptibility of the three $(FA)_2PF_6$ single crystals used in this contribution for the analysis of the influence of defects on the conduction-electron spin diffusion. In these quasi-1D conductors, the influence of the charge-density-wave fluctuations giving rise to a pseudogap of $\Delta_{eff}(T)\approx25-35$ meV and

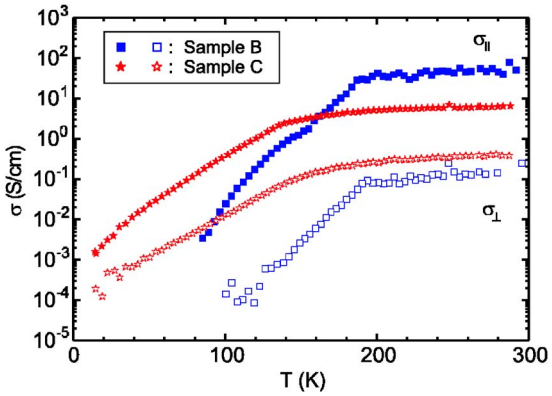

FIG. 1. (Color online) Microwave conductivity (10 GHz) for two $(FA)_2PF_6$ single crystals of varying defect content (crystals B and C of Table I) parallel or perpendicular to the stacking direction.

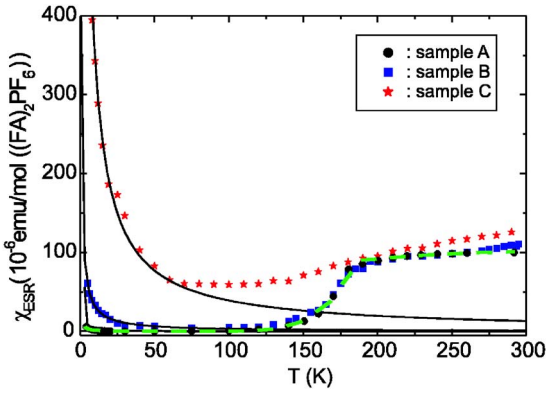

FIG. 2. (Color online) Temperature dependence of the paramagnetic susceptibility (ESR intensity) of the $(FA)_2PF_6$ single crystals *A*, *B*, and *C* (Table I). The low-temperature Curie tail, approximated by the solid-line C/T fit, is used to estimate the tabulated defect content x. Its subtraction leaves the conduction-electron contribution (broken line for crystal *A*) (Ref. 26).

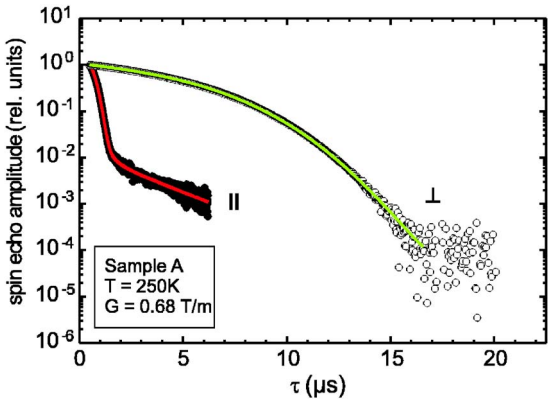

FIG. 3. (Color online) Decay of the conduction electron spin echo for the highest-purity sample *A* (Table I), for magnetic field gradient parallel or perpendicular to the stacking axis *a* (9.6 GHz, G=0.68 T/m, T=250 K). The solid line shows the fit according to Sec. II, yielding the parameters visualized in Figs. 5–7 below.

reducing the density of states at the Fermi level, $N(E_F,T)$, in the metallic phase, can be monitored by the temperature dependence of the magnetic susceptibility.[26] Likewise, the opening of the static energy gap below T_P has been derived "magnetically," with $\Delta(0)=50-90$ meV (full gap$=2\Delta$). Quantitative interpretation of the electrical conductivity parallel to the FA stacks could be given in a semiconductorlike framework, using the magnetically derived effective or real gap and taking the acoustic deformation potential scattering into account.[27,28]

The anisotropy of the mobility and the defect-induced scattering of the charge and spin carriers can be monitored more specifically. Guided by the Einstein relation for the electrical conductivity $\sigma(T)$,

$$\sigma(T) = e^2 N(E_F,T) D(T), \tag{1}$$

the experiment can be focused on the direct derivation of the diffusion coefficients $D_\parallel(T)$ and $D_\perp(T)$, separating thus the temperature-dependent influence of the real or pseudogap on the density of states.[29–31] It has been shown recently that indeed the electric current in $(FA)_2PF_6$ can be detected by ESR via the motion of the spins in a magnetic field gradient.[32] Thus the experimental techniques established earlier for the derivation of the spin diffusion coefficient $D(T)$, its anisotropy $D(\theta)$, and the spatial restriction of spin diffusion due to broken chains or exchange interaction with paramagnetic defects, $l_\parallel(T)$, can be adopted.[29–31,33–43] This is exploited here for different $(FA)_2PF_6$ single crystals with controlled content of defects, allowing extrapolation to the behavior of ideal $(FA)_2PF_6$ crystals.

This paper is organized as follows. The theoretical relations required to derive the diffusion coefficients $D_\parallel(T)$ and $D_\perp(T)$, the characteristic chain length $l_c(T)$ of the chain length distribution, and the transverse spin relaxation times $T_{2\parallel}(T)$ and $T_{2\perp}(T)$ are summarized in Sec. II. Samples and instrumentation are described in Sec. III. The results, presented in Sec. IV A, are discussed and quantitatively interpreted in Sec. IV B, followed by concluding remarks in Sec. V.

II. THEORETICAL BASIS FOR THE ANALYSIS

The ESR measurement of the conduction-electron spin diffusion coefficients $D_\parallel(T)$ and $D_\perp(T)$ is based on the relations established by Torrey, Stejskal, and Tanner for the derivation of self-diffusion coefficients in nuclear magnetic resonance.[44,45] The attenuation of the spin echo at $t=2\tau$, excited by a 90°-τ-180° pulse sequence, follows for free diffusion in a magnetic field gradient G_z the relation

$$\frac{A(2\tau)}{A(0)} = \exp\left(-\frac{2\tau}{T_2} - \frac{2}{3} D_z \gamma^2 G_z^2 \tau^3\right). \tag{2}$$

This "free-diffusion limit" is appropriate for the motion of the conduction electrons perpendicular to the highly conducting direction in arene radical cation salts. It has to be considered, however, that the transverse relaxation time T_2 depends on field orientation, temperature, frequency, and defect contribution of the individual single crystal.[46–48] Because there is a spatial variation of the impurity concentration in most electrochemically grown crystals, there is also a distribution of T_2 times in these crystals.[19,37] By variation of the magnetic field gradient $G_z=G_\perp$ the two contributions in Eq. (2) can nevertheless be separated and reliable values of $D_\perp(T)$ are obtained.[49]

Analysis of the spin diffusion coefficient parallel to the preferred direction, $D_\parallel(T)$, is much more complicated, because its absolute value is so large that the free-diffusion length

$$l_D = (2D_\parallel t)^{1/2} \tag{3}$$

within a typical pulsed ESR experiment ($t \leq 20$ μs) would be larger than the average separation of extended obstacles, l, of crystals that are not specifically selected for low content of paramagnetic defects (caused, e.g., by local deviation from 2:1 stoichiometry) or the absence of any extended cracks

(caused, e.g., by sample handling or too rapid temperature cycles). It has been shown, however, that the chain length distribution can be approximated by an exponential function[33,34,40]

$$p(l) = l_c^{-1}\exp(-l/l_c) \tag{4}$$

giving the weight factor for the contribution of the conduction-electron spins in a finite chain segment of length l

$$P(l) = l/l_c^{-2}\exp(-l/l_c). \tag{5}$$

Thus, only one parameter has to be adjusted for the fit to the experiment, termed the "characteristic chain length" l_c. Conduction electrons in channels of length l_c predominate in the ESR signal. Experiments indicated that the walls of the finite channels are typically highly reflecting, and only weakly relaxing.[34,39,41]

For the fit of the spin echo decay $M(2\tau)/M(0)$ by

$$\frac{M(2\tau)}{M(0)} = \frac{A(l,2\tau)}{A(l,0)} \otimes P(l), \tag{6}$$

folding of the length distribution $P(l)$ with the appropriate echo decay function, modified with respect to Eq. (2) on account of the finite chain length l, has to be performed self-consistently.[40,50] The particular chain length l has to be compared with l_D [Eq. (3)] and the dephasing length l_G, given by[51,52]

$$l_G = (6\pi/\gamma G)^{1/3}. \tag{7}$$

Only for $l_D \ll l_G$ and l, the free-diffusion limit of Eq. (2) can be used in Eq. (6). An analytical expression has been derived for the motional narrowing regime $l \ll l_D, l_G$,[53,54]

$$\frac{A(l,2\tau)}{A(l,0)} = \exp\left(-\frac{2\tau}{T_2}\right)\exp\left[-\frac{8\gamma^2G^2l^4}{D\pi^6}\sum_{n=0}^{\infty}\frac{1}{(2n+1)^6}\left(2\tau - \frac{3-4e^{-Q\tau}+e^{-2Q\tau}}{Q}\right)\right], \tag{8}$$

with $Q = D(2n+1)^2\pi^2/l^2$. In the so-called localization regime, for long times, large gradients, and long chains ($l_G \ll l, l_D$), enhancement of the signals from close to the reflecting walls is observed, which can be approximated by the exponential decay[51,52]

$$\frac{A(l,2\tau)}{A(l,0)} = \frac{c}{l}\left(\frac{D}{\gamma G}\right)^{1/3}\exp\left(-\frac{2\tau}{T_2}\right)\exp[a_1(D\gamma^2G^2)^{1/3}\tau] \tag{9}$$

with $c \approx 5.8841$ and $a_1 \approx -1.0188$. Fortunately, the self-consistent fitting routines were established earlier already,[50] and just had to be applied to the measurements presented below.

III. EXPERIMENTAL DETAILS

A. Sample preparation

Single crystals of $(FA)_2PF_6$ were grown at $T=-30$ °C by standard electrocrystallization techniques, using platinum electrodes and methyl formate as solvent.[13–15] For the highest-purity samples, special care was taken in the zone refinement of the fluoranthene starting material and the number of recrystallizations of the tetrabutylammonium-PF_6 salt. The actual "purity" was controlled via the low-temperature Curie law contribution (Fig. 2) of the magnetic susceptibility.[26] It is given as the total concentration x of localized spin $S=1/2$ defects per formula unit $(FA)_2PF_6$ in Table I. Deviations from exact 2:1 stoichiometry, chains that are not multiples of four FA molecules long, breaking, and aging defects (crystal decomposition) all add up to the given x value.[47,55] In order to realize a high defect concentration $x=1.1\%$, the respective crystal was irradiated with a high-energy proton beam to a dose of up to 5.4×10^{16} protons per cm^2 at room temperature ($E_p=25$ MeV, $t=0.75$ h, $I=0.1$ μA).[39,40] Under such conditions, the Peierls transition temperature of $(FA)_2PF_6$ is lowered substantially, to $T_P=131.5$ K.[43] It has been shown before that the Peierls transition in arene radical cation salts can be suppressed by disorder in the anion channel.[56] This results from the role played by the anions in coupling the 1D CDW fluctuations.[18,57] The radiation-induced defects and disorder may be supposed to act in the same way. It has been shown by Overhauser-shift-detected proton spin lattice relaxation, however, that only some of the radiation defects interact with the conduction electrons in the FA stack.[58]

TABLE I. Sample characteristics of $(FA)_2PF_6$ single crystals A, B, and C, where sample C was proton irradiated. x is the number of Curie paramagnetic $S=1/2$ defects per formula unit, T_P the Peierls temperature, derived from $d(\ln\sigma_\parallel)/d(1/T)$, and L the sample dimensions parallel and perpendicular to FA stacking axis a.

Sample	x	T_P (K)	$L_\parallel \times L_\perp \times L'_\perp$ (mm^3)
A	7.2×10^{-5}	186	$0.60\times0.60\times0.40$
B	9.0×10^{-4}	180	$0.61\times0.22\times0.22$
C	1.1×10^{-2}	131.5	$1.1\times0.37\times0.35$

Before being used for the diffusion coefficient measurements, all crystals were controlled for twinning or pronounced growth sectors by X-band continuous-wave ESR. In addition, except for the most perfect crystal (A), the microwave conductivity was measured parallel and perpendicular to the FA stacks at 10 GHz during slow cooling of the crystals (Fig. 1).[43,59] For further reference, the data of the crystals used below are compiled in Table I.

B. Pulsed ESR measurements

Spin echo decay in a well-defined magnetic field gradient was measured at the X band (9.6 GHz) using a Bruker ELEXSYS E-580 FT-EPR spectrometer with dielectric resonator and ER 4118 CF He gas-flow-cooled metal cryostat. Spin echos were excited by 90° and 180° pulses of 16 and 32 ns, respectively. A 16-step phase cycle was used, and up to 1024×16 scans were accumulated. The magnetic field gradient of appropriate fixed strength parallel to the main field direction was realized by two iron wedges on one of the pole caps of the electromagnet. The respective gradient was cali-

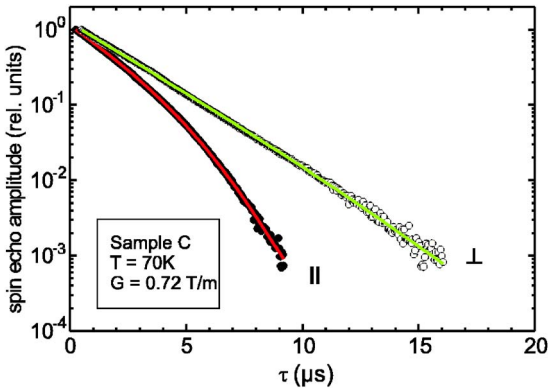

FIG. 4. (Color online) Low-temperature conduction-electron spin echo decay for the most defect-rich (proton-irradiated) sample *C* (Table I), for magnetic field gradient parallel and perpendicular to the stacking axis *a* (9.6 GHz, $G=0.72$ T/m, $T=70$ K). The Peierls transition of sample *C* was observed at $T_P=131.5$ K. The solid line shows the fit according to Sec. II (see Figs. 5–7).

brated by ESR measurement. Due to the extreme anisotropy of $D(\theta)$, it was of crucial importance for the possibility to determine undisturbed values of the small coefficient $D_\perp(T)$ that the field profile in the directions perpendicular to the main gradient direction was controlled experimentally as well.[40] Thus the sample could be positioned at the place with minimal interference of unwanted gradients [mixing $D_\parallel(T)$ into the supposed $D_\perp(T)$ measurement]. In order to minimize such artifacts further, only short segments of the crystals ($L_\parallel \approx 140$ μm) were used for the $D_\perp(T)$ data recording. A dual-axis goniometer was used to adjust the sample along the two extreme orientations of $D_\parallel$ and $D_\perp$ empirically. Figure 3 shows a typical example for the difference in the spin echo decay for magnetic field and field gradient parallel, or perpendicular, to the preferred direction for the metallic phase of the high-purity sample *A*. For the perpendicular orientation, free diffusion (with $D_\perp$) and relaxation give rise to the slow echo decay over four orders of magnitude, where the noise level is reached. On the other hand, for the parallel orientation, already after the decay by two orders of magnitude caused by the fast diffusion ($D_\parallel$), transition to slower,

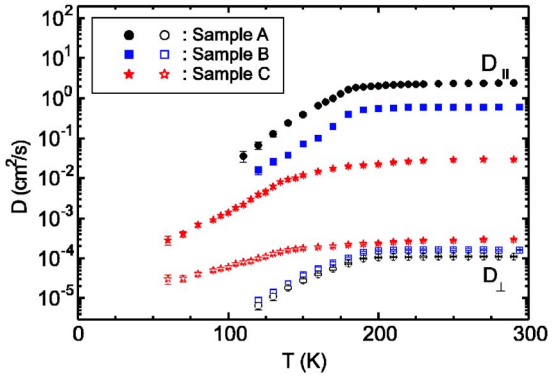

FIG. 5. (Color online) Temperature dependence of the diffusion coefficients $D_\parallel$ and $D_\perp$ for the three $(FA)_2PF_6$ single crystals *A*, *B*, and *C* characterized in Table I. For fit parameters for Eqs. (10) and (11) see Table II.

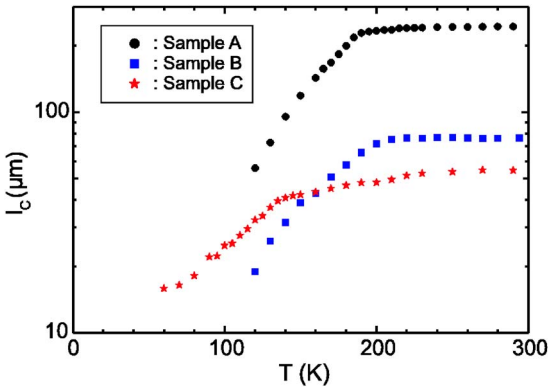

FIG. 6. (Color online) Temperature dependence of the characteristic chain length l_c for the samples *A*, *B*, and *C*. For fit parameters, using Eqs. (10) and (11) see Table II.

approximately exponential decay can be seen in Fig. 3. For comparison, Fig. 4 shows the much smaller difference for lower temperature and the sample with the largest concentration of defects. The corresponding fit using the relations outlined in Sec. II is shown as solid line. Perfect agreement could be achieved for all samples and temperatures and both orientations, resulting in the $D(T)$, $l_c(T)$, and $1/T_2$ data presented in Figs. 5–7, respectively. It should be mentioned that, in principle, in addition to the chain length distribution considered for the fit, a distribution of T_2 values has to be accepted. However, we showed in the past via comparison of 3D spatially resolved relaxation measurements with integral average data that the variation by typically a factor of 2 within one crystal can reasonably be replaced by one average value.[60] In this regard, the values of D and $1/T_2$ plotted in Figs. 5 and 7 are "effective" values.

IV. EXPERIMENTAL RESULTS AND DISCUSSION

A. Experimental results

In the temperature dependence of the quantities visualized in Figs. 1, 2, and 5–7 for the $(FA)_2PF_6$ crystals *A*, *B*, and *C*,

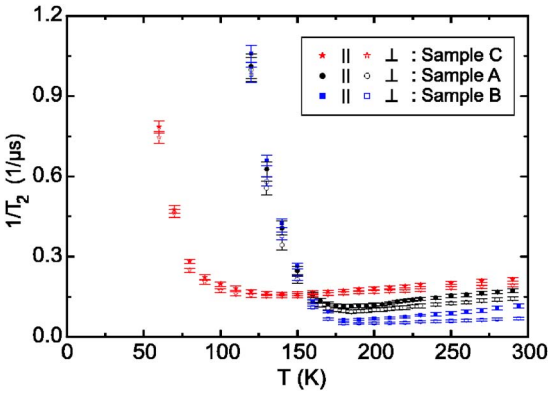

FIG. 7. (Color online) Temperature dependence of the transverse relaxation rates $(T_{2,\parallel})^{-1}$ and $(T_{2,\perp})^{-1}$ for the three $(FA)_2PF_6$ single crystals *A*, *B*, and *C* characterized in Table I, shown as filled and open symbols, respectively.

TABLE II. Experimental data (T=250 K) and fit parameters. Activated behavior and power law are adjusted alternately [Eqs. (10) and (11)].

	Sample		
	A	*B*	*C* (*p* irradiated)
$\sigma_{\parallel}$ (250 K) (S/cm)		42.4(6)	5.95(6)
$\Delta E_{\parallel,HT}$ (meV)		26(4)	14(1)
$\Delta E_{\parallel,LT}$ (meV)		248(19)	56(1)
$\alpha_{\parallel,HT}$		1.3(2)	0.7(1)
$\alpha_{\parallel,LT}$		16.2(5)	5.7(1)
$\sigma_{\perp}$ (250 K) (S/cm)		0.149(4)	0.362(5)
$\Delta E_{\perp,HT}$ (meV)		43(7)	25(1)
$\Delta E_{\perp,LT}$ (meV)		199(3)	49(2)
$\alpha_{\perp,HT}$		2.1(3)	1.3(1)
$\alpha_{\perp,LT}$		13.4(1)	5.1(1)
ΔE_{χ} (meV)	92(1)	69(1)	19(1)
α_{χ}	9.24(36)	5.65(14)	2.16(11)
$T_{2,\parallel}$ (250 K) (μs)	6.5(3)	11.2(4)	5.0(3)
$D_{\parallel}$ (250 K) (cm^2/s)	2.35(7)	0.61(6)	0.030(2)
$\Delta E_{\parallel,HT}$ (meV)	9.6(9)	6.0(9)	17.7(9)
$\Delta E_{\parallel,LT}$ (meV)	102(3)	86(10)	52(3)
$\alpha_{\parallel,HT}$	0.5(1)	0.3(1)	0.9(1)
$\alpha_{\parallel,LT}$	7.44(19)	7.06(60)	5.31(20)
l_c(250 K) (μm)	243(1)	77.7(6)	53.6(5)
$\Delta E_{c,LT}$ (meV)	39(1)	32.5(1.0)	17.5(1.0)
$\alpha_{c,LT}$	2.87(5)	2.5(1)	1.6(1)
$T_{2,\perp}$ (250 K) (μs)	7.9(3)	16.8(4)	5.4(3)
$D_{\perp}$ (250 K) (cm^2/s)	$1.1(3)\times10^{-4}$	$1.6(1)\times10^{-4}$	$3.0(1)\times10^{-4}$
$\Delta E_{\perp,HT}$ (meV)	2.6(3)	3.8(9)	14.7(7)
$\Delta E_{\perp,LT}$ (meV)	78(1)	69(2)	30(2)
$\alpha_{\perp,HT}$	0.12(1)	0.18(9)	0.83(6)
$\alpha_{\perp,LT}$	5.48(8)	5.0(1)	2.59(11)

the Peierls transition at T_P (Table I) can easily be seen, especially clearly for the most perfect sample *A*. $\sigma_{\parallel}(T)$ (Fig. 1), $\chi_{ESR}(T)$ (Fig. 2), $D_{\parallel}(T)$ (Fig. 5), and $l_c(T)$ (Fig. 6) all show a break in slope at T_p. For the transverse electron spin relaxation rate $1/T_2$, T_p concides with its minimum (Fig. 7). Rounding of the anomalies is observed with increasing defect content x. Nevertheless, high-temperature (HT) and low-temperature (LT) range can clearly be distinguished, and compared with simplified analytical temperature dependences. Evidently, and in agreement with Eq. (1), the microwave electrical conductivity varies by more orders of magnitude than the diffusion coefficient below T_P in the same temperature range (Fig. 5 versus Fig. 1). Instrumentally, a larger anisotropy can be shown for $D_{\parallel}:D_{\perp}$ than for $\sigma_{\parallel}:\sigma_{\perp}$ because the demagnetizing field is negligible in $(FA)_2PF_6$ and therefore does not spoil the homogeneity of the external magnetic field and gradient applied along the principal directions $\parallel$ and $\perp$. In contrast the homogeneity of the microwave electrical field is influenced for the nonellipsoidal sample shape in the metallic phase (skin effect regime) by electric depolarizaton, and thus the ratio $\sigma_{\parallel}:\sigma_{\perp}$ is reduced. It has been shown that when the static energy gap opens at the Peierls transition temperature T_p, its temperature dependence $\Delta(T)$ can be derived by quantitative analysis of the magnetic susceptibility.[26] However, with useful accuracy the resulting temperature dependence of the respective thermally activated physical quantity $\chi(T)$ could also be parametrized in the temperature range $T_p/2 \leq T \leq T_p$ by an activation law adjusting an effective T-independent activation energy ΔE [which turned out to be about twice as large as $\Delta(0)$ in $(FA)_2PF_6$].[26] This "effective" role of all low-temperature parameters compiled in Table II has to be kept in mind. It in no way reduces their usefulness for a comparison of anisotropies or sample dependences.

Figure 5 shows the anisotropy and temperature dependence of the conduction-electron spin diffusion coefficient for the three $(FA)_2PF_6$ single crystals *A*, *B*, and *C* characterized in Table I. The most pronounced variation is observed for motion parallel to the stack. $D_{\parallel}$ is reduced by a factor of 80 for an increase of the defect concentration x by a factor of 150. By contrast, $D_{\perp}$ increases with defect concentration x, even if only by a smaller factor. Below the respective Peierls

transition temperature T_P, the more pronounced dependence of $D(T)$ can reasonably be described by a thermally activated behavior

$$D(T) = D_\infty \exp(-\Delta E/k_B T) \tag{10}$$

as well as by a power law

$$D(T) = D(T_P)(T/T_P)^\alpha \tag{11}$$

with the most relevant fit parameters compiled in Table II. Obviously a weaker temperature dependence is observed for the direction perpendicular to the stack than for that parallel to the stack. For further discussion also the fit parameters ΔE and α for a description of the temperature dependence of $\sigma_\parallel(T)$, $\sigma_\perp$, and $\chi_{c.e.}(T)$ using Eqs. (10) and (11) are given in Table II.

The variation of the characteristic chain length l_c is shown in Fig. 6. For sample A, in the HT range, the characteristic chain length $l_c \approx 250$ μm is long enough to allow free diffusion from one end of the crystal A to the other for a relevant portion of the one-dimensional chains. The reduction of l_c with increasing defect concentration x in the metallic phase is undisputable, but comparing samples B and C the reduction factor of l_c is smaller than that of $\sigma_\parallel$ or $D_\parallel$, and especially smaller than the ratio of the defect concentrations x. This is in accordance with a recent analysis of proton spin lattice relaxation via the Overhauser shift technique that indicated a nonuniform distribution of the proton-irradiation-induced defects in sample C.[58] A relevant part of the defects (x) in this sample seems to reside on the crystal's surface, and has therefore only a minor influence on the conduction-electron spins characterized by the pulsed ESR experiment. A steeper decrease of $l_c(T)$ is observed below the structural phase transition, $T < T_S$, and it is even more pronounced below the Peierls transition, $T < T_P$. The fit parameters required for an analytical description in analogy to Eqs. (10) and (11), are again collected in Table II.

Figure 7 represents the transverse relaxation rates $1/T_2$ of the three single crystals, derived from the fits along Sec. II. In agreement with earlier results, $1/T_2$ is larger for magnetic field parallel to the stacking direction than for the perpendicular orientation, which is caused by the angular dependence of intrastack dipolar interactions between conduction-electron and localized-defect-electron spins. The relaxation rate $1/T_2$ increases weakly above T_p with increasing temperature in the metallic phase of all three $(FA)_2PF_6$ crystals, but increases strongly if the temperature is lowered below T_P. At fixed temperature in the metallic phase, $1/T_2$ decreases with increasing, but low defect concentration x (from sample A to B), but increases again for the higher defect content of the proton-irradiated sample C. This nonmonotonic variation follows from the interplay of the three different contributions to $1/T_2$: (i) the hyperfine interaction, (ii) the intrastack dipole-dipole and exchange interactions between defect and conduction electron spins in the presence of a bottleneck situation for the spin lattice relaxation,[46–48] and (iii) the spin-orbit scattering contribution (Elliott mechanism) of the conduction electrons, which is strongly suppressed in perfect one-dimensional conductors, but is reestablished by irradiation-induced defects and segmentation of chains.[61–63] T_2 data for $T=250$ K are again included in Table II.

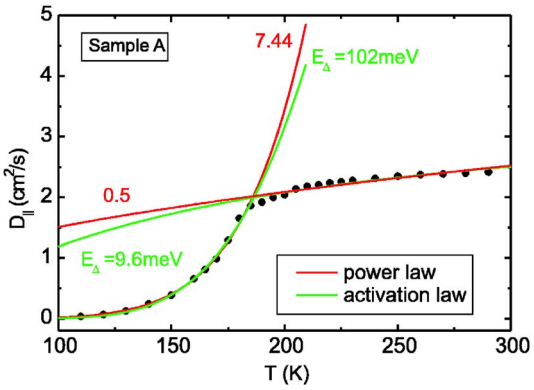

FIG. 8. (Color online) Temperature dependence of the diffusion coefficient $D_\parallel(T)$ of sample A in comparison with activation and power-law fits (Table II).

Discussion of the applicability of the Luttinger liquid model to quasi-one-dimensional conductors with CDW fluctuations requires experimental data for the high-temperature metallic phase of the $(FA)_2PF_6$ crystals. As far as accessible, corresponding HT fit parameters for Eqs. (10) and (11) are included in Table II. The temperature dependence of the various quantities can only be examined using Eqs. (10) and (11) in relatively narrow ranges of about $T_p/2-T_p$ in the LT range and T_p-2T_p in the HT range. Therefore, reasonable agreement is observed for both versions of the analytical description, as is exemplified in Fig. 8 for the diffusion coefficient $D_\parallel(T)$ of sample A.

B. Discussion

A semiconductor-like description of magnetic susceptibility and dc as well as microwave conductivity of $(FA)_2PF_6$ crystals was established in the past.[26–28] A barely temperature-dependent pseudogap $2\Delta_{eff}(T)$ was able to describe the fluctuations around the Peierls transition in the HT metallic phase, and the accompanying temperature-dependent reduction of the effective density of states at the Fermi energy, $N(E_F,T)$. On the other hand, the static energy gap $\Delta(T)$ was observed to increase in BCS-like fashion below the Peierls transition, reaching a constant value $2\Delta(0)$ only at $T \ll T_p$. Thus the description of other physical quantities like $D(T)$ or $l_c(T)$ in the HT range T_p-2T_p by an activation law is in line with these earlier results, whereas the description of the LT quantities in the $T_p/2-T_p$ range by a fixed value of ΔE_{LT} can only give a qualitative, phenomenological parametrization. It is helpful for a comparison of the temperature dependences of the three samples A, B, and C with well-defined differences in the defect concentrations, nevertheless.

In the framework of the Luttinger liquid description of one-dimensional conductors, power-law descriptions, and relations between the exponents describing different quantities have been introduced.[64,65] This was the driving force to fit also Eq. (11) to the temperature dependencies observed in the current investigation. We can use the parameters α com-

piled in Table II in order to question the consistency of this power-law description.

1. Consistency of power-law parameters

For a Luttinger liquid a power law with the Fermi surface exponent $\alpha_{Lu}=(1/4)(K_\rho+(1/K_\rho)-2)$ is expected, where K_ρ describes the interaction of the electrons ($K_\rho=1$ corresponds to no interactions). For $(FA)_2PF_6$ with a half filling of the conduction band due to a 2:1 stoichiometry with, however, the formation of dimers of the noncentrosymmetric FA molecules stacked with 180° rotation, one gets the following expressions for the dc conducting regime: $\sigma_\parallel(T)\propto T^{3-4K_\rho}$ and $\sigma_\perp\propto T^{2\alpha_{Lu}-1}$. Using the power-law-fitted values, obtained by temperature-dependent $\sigma_\perp$ and $D_\perp$ measurements (Table II), the exponent α_{Lu} as well as K_ρ could be calculated. With these computed constants the theoretical $\sigma_\parallel$ and $D_\parallel$ temperature dependence (i.e., $\propto T^{3-4K_\rho}$) was evaluated. For all samples and all diffusion and conductivity measurements the exponent so obtained for temperature dependence differs drastically from the fitted data. Also the calculated values of α_{Lu} and K_ρ are quite out of range of the theoretical predictions and experimental results for other quasi-one-dimensional systems like $TMTTF_2PF_6$ (TMTTF: tetramethyltetrathiofulvalene).[64]

Due to this disagreement there is no real evidence that the conduction electrons in the $(FA)_2PF_6$ compounds can be considered as a Luttinger liquid. In regard to the relative role of electron-electron and electron-phonon interaction this seems to be quite reasonable, in contrast with the Bechgaard salts. The predominating electron-phonon interaction favors evidently a semiconductorlike description of the arene radical cation salts.

2. Influence of defects

The comparison of the three $(FA)_2PF_6$ single crystals with varied content of low-temperature Curie paramagnetic defects reveals clearly the systematics of the defect-induced changes in a highly one-dimensional organic conductor with charge-density-wave fluctuations in the metallic phase and a commensurate CDW Peierls distorted low-temperature phase. First of all, the Curie tail in the low-temperature magnetic susceptibility grows (Fig. 2). Second, the Peierls transition shifts to lower temperature and the accompanying anomalies in σ,χ, and D are rounded. The activation energies of $\sigma_\parallel(T),\chi(T)$, and $D_\parallel(T)$ in the LT phase are lowered with increasing defect content. In the metallic HT phase, the absolute values of microwave conductivity $\sigma_\parallel(T)$, conduction-electron spin diffusion coefficient $D_\parallel(T)$, and characteristic chain length $l_c(T)$ (for the restricted diffusion of the conduction electron spins) are reduced strongly with increasing defect content, because conduction electrons have to leave their one-dimensional chain in order to bypass these defects. The characteristic chain length derived via the analysis of the conduction-electron spin echo decay decreases generally below the structural and even more so below the Peierls transition. It seems to reflect the typical space that is still available for leftover conduction electrons in the LT phase. The decay of $l_c(T)$ below T_p is less abrupt for the crystals with larger defect content.

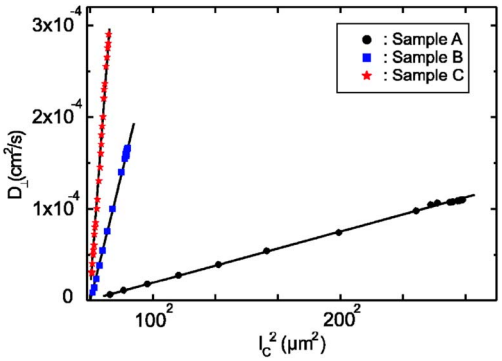

FIG. 9. (Color online) Visualization of the linear correlation between diffusion coefficient $D_\perp(T)$ and square of the characteristic chain length, $[l_c(T)]^2$, for samples *A*, *B*, and *C*.

For the $(FA)_2PF_6$ crystal with the highest purity, anisotropy of the diffusion coefficient $D_\parallel(250\ \mathrm{K})/D_\perp(250\ \mathrm{K})\approx 2\times 10^4$ is observed. Extrapolation to vanishing defect content of an ideal $(FA)_2PF_6$ crystal indicates an intrinsic anisotropy of $D_\parallel:D_\perp\approx 45\,000$. The anisotropy of the microwave conductivity and diffusion coefficient is reduced severely with increasing defect content. $\sigma_\perp(T)$ and $D_\perp(T)$ clearly increase with growing defect content of the crystal, though by a smaller factor than is observed for the decrease of the corresponding parallel components. Defects evidently favor the transverse electron spin and charge motion. It is interesting to note and currently unexplained that the perpendicular-to-stack diffusion coefficient $D_\perp(T)$ of the various crystals increases in the LT and HT phases correlated with the square of the characteristic chain length $l_c(T)$ (Fig. 9). That the length of the channel that is available for the unrestricted motion of the conduction electron along the stack favors the perpendicular motion is an argument against incoherent perpendicular hopping motion of the conduction-electron spins.

V. CONCLUDING REMARKS

The various results presented for three individual single crystals of the one-dimensional organic conductor $(FA)_2PF_6$ with varied defect content support the description of the microwave electrical conductivity as a product of a temperature-dependent density of states and temperature-dependent spin diffusion coefficient $D(T)$. For the highest-purity crystal (*A*) an anisotropy of $D_\parallel/D_\perp\approx 2\times 10^4$ is observed in the metallic phase, only about a factor of 2 lower than the extrapolated intrinsic anisotropy. The influence of the defect concentration on the relevant physical quantities has been estabished above as well as below the Peierls transition temperature. No arguments for a distinction of charge and spin motion have been found.

ACKNOWLEDGMENTS

We thank S. Matejcek, D. Stöffler, A. Warth, and T. Wokrina for experimental contributions and M. Drescher and N. Kaplan for discussions. This project was financially supported by the Deutsche Forschungsgemeinschaft (Grant No. Do181/10-3).

[1] *Proceedings of the International Workshop on Electronic Crystals, ECRYS-2005*, edited by S. Brazovskii, P. Monceau, and N. Kirova [J. Phys. IV **131**, 1 (2005)].
[2] S. V. Zaitsev-Zotov, Microelectron. Eng. **69**, 549 (2003).
[3] S. V. Zaitsev-Zotov, Phys. Usp. **47**, 533 (2004).
[4] S. N. Artemenko and S. V. Remizov, Phys. Rev. B **72**, 125118 (2005).
[5] Yu. Lu, *Solitons and Polarons in Conducting Polymers* (World Scientific, Singapore, 1988).
[6] A. J. Heeger, S. Kivelson, J. R. Schrieffer, and W.-P. Su, Rev. Mod. Phys. **60**, 781 (1988).
[7] S. Brazovskii and N. Kirova, Sov. Sci. Rev., Sect. A **5**, 99 (1984).
[8] Z. Vardeny, E. Ehrenfreund, J. Shinar, and F. Wudl, Phys. Rev. B **35**, 2498 (1987).
[9] Yu. I. Latyshev, P. Monceau, S. Brazovskii, A. P. Orlov, and T. Fournier, Phys. Rev. Lett. **95**, 266402 (2005).
[10] S. Brazovskii, cond-mat/0606009 (unpublished).
[11] W. Rieß and W. Brütting, Phys. Scr., T **49**, 721 (1993).
[12] V. Ilakovac, S. Ravy, J. P. Pouget, W. Rieß, W. Brütting, and M. Schwoerer, J. Phys. (Paris), Colloq. **3**, C2-137 (1993).
[13] C. Kröhnke, V. Enkelmann, and G. Wegner, Angew. Chem. **92**, 941 (1980).
[14] V. Enkelmann, B. S. Morra, Ch. Kröhnke, G. Wegner, and J. Heinze, Chem. Phys. **66**, 303 (1982).
[15] V. Enkelmann, Adv. Chem. Ser. **217**, 177 (1988).
[16] V. Enkelmann and K. Göckelmann, Ber. Bunsenges. Phys. Chem. **91**, 950 (1987).
[17] Th. Schimmel, W. Rieß, G. Denninger, and M. Schwoerer, Ber. Bunsenges. Phys. Chem. **91**, 901 (1987).
[18] K. S. Lee, D.-K. Seo, J. Ren, M.-H. Whangbo, S. N. Magonov, G. Bar, and W. Brütting, Synth. Met. **80**, 1 (1996).
[19] C. Buschhaus, J. Gmeiner, H. Henke, M. Ulrich, and E. Dormann, Synth. Met. **149**, 89 (2005).
[20] Th. Schimmel, B. Koch, H. P. Geserich, and M. Schwoerer, Synth. Met. **33**, 311 (1989).
[21] W. Brütting, W. Rieß, and M. Schwoerer, Ann. Phys. **1**, 409 (1992).
[22] C. Hauenschild, H. W. Helberg, W. Rieß, W. Brütting, and M. Schwoerer, Synth. Met. **55-57**, 2635 (1993).
[23] W. Brütting, G. Witt, A. Rötger, and W. Rieß, Synth. Met. **70**, 1303 (1995).
[24] D. Berner, V. M. Burlakov, G. Scheiber, K. Widder, H. P. Geserich, J. Gmeiner, and M. Schwoerer, Solid State Commun. **97**, 863 (1996).
[25] G. Sachs, W. Stöcklein, B. Bail, E. Dormann, and M. Schwoerer, Chem. Phys. Lett. **89**, 179 (1982).
[26] U. Köbler, J. Gmeiner, and E. Dormann, J. Magn. Magn. Mater. **69**, 189 (1987).
[27] P. H. Nguyen, G. Paasch, W. Brütting, and W. Rieß, Phys. Rev. B **49**, 5172 (1994).
[28] W. Brütting, P. H. Nguyen, W. Rieß, and G. Paasch, Phys. Rev. B **51**, 9533 (1995).
[29] G. G. Maresch, A. Grupp, M. Mehring, J. U. von Schütz, and H. C. Wolf, J. Phys. I **46**, 461 (1985).
[30] M. Mehring, in *Low-Dimensional Conductors and Superconductors*, edited by D. Jerome and L. G. Caron (Plenum Publishing, New York, 1987), p. 185.
[31] R. Ruf and E. Dormann, Z. Phys. B: Condens. Matter **102**, 157 (1997).
[32] M. Drescher, N. Kaplan, and E. Dormann, Phys. Rev. Lett. **96**, 037601 (2006).
[33] R. Ruf, N. Kaplan, and E. Dormann, Phys. Rev. Lett. **74**, 2122 (1995); **75**, 1237 (1995); E. Dormann and N. Kaplan, *ibid.* **76**, 334 (1996).
[34] N. Kaplan, E. Dormann, R. Ruf, A. Coy, and P. T. Callaghan, Phys. Rev. B **52**, 16385 (1995).
[35] T. Wokrina, E. Dormann, and N. Kaplan, Europhys. Lett. **49**, 244 (2000).
[36] G. Alexandrowicz, T. Tashma, A. Feintuch, A. Grayevsky, E. Dormann, and N. Kaplan, Phys. Rev. Lett. **84**, 2973 (2000).
[37] T. Tashma, A. Feintuch, A. Grayevsky, J. Gmeiner, A. Gabay, E. Dormann, and N. Kaplan, Synth. Met. **132**, 161 (2003).
[38] A. Feintuch, A. Grayevsky, C. Buschhaus, E. Dormann, and N. Kaplan, Curr. Appl. Phys. **4**, 373 (2004).
[39] T. Wokrina, J. Gmeiner, N. Kaplan, and E. Dormann, Phys. Rev. B **67**, 054103 (2003).
[40] T. Wokrina, J. Gmeiner, N. Kaplan, and E. Dormann, Eur. Phys. J. B **35**, 191 (2003).
[41] A. Feintuch, A. Grayevsky, N. Kaplan, and E. Dormann, Phys. Rev. Lett. **92**, 156803 (2004).
[42] M. Drescher, N. Kaplan, and E. Dormann, Phys. Rev. Lett. **94**, 016404 (2005).
[43] M. Drescher, D. Saez de Jauregui, S. Matejcek, and E. Dormann, Synth. Met. **152**, 401 (2005).
[44] H. C. Torrey, Phys. Rev. **104**, 563 (1956).
[45] J. E. Tanner and E. O. Stejskal, J. Chem. Phys. **49**, 1768 (1968).
[46] G. Sachs, E. Pöhlmann, and E. Dormann, J. Magn. Magn. Mater. **69**, 131 (1987).
[47] E. Dormann and G. Sachs, Ber. Bunsenges. Phys. Chem. **91**, 879 (1987).
[48] B. Pongs and E. Dormann, J. Phys.: Condens. Matter **15**, 5121 (2003).
[49] A. Warth, D. Saez de Jauregui, and E. Dormann, J. Phys.: Condens. Matter **17**, 4825 (2005).
[50] T. Wokrina, Ph.D. thesis, Universität Karlsruhe (TH), 2002.
[51] M. D. Hürlimann, K. G. Helmer, T. M. de Swiet, P. N. Sen, and C. H. Sotak, J. Magn. Reson., Ser. A **113**, 260 (1995).
[52] T. M. de Swiet and P. N. Sen, J. Chem. Phys. **100**, 5597 (1994).
[53] C. H. Neumann, J. Chem. Phys. **60**, 4508 (1974).
[54] B. Robertson, Phys. Rev. **151**, 273 (1966).
[55] G. Sachs and E. Dormann, Synth. Met. **25**, 157 (1988).
[56] C. Buschhaus, R. Desquiotz, K. Eichhorn, M. Hofmann, K. Hümmer, V. Illich, M. Kelemen, S. Tarragona Auga, T. Wokrina, A. Zitsch, and E. Dormann, Eur. Phys. J. B **8**, 57 (1999).
[57] A. Kaiser and E. Dormann, Phys. Rev. B **71**, 115108 (2005).
[58] D. Stöffler, M. Drescher, D. Saez de Jauregui, J. Gmeiner, and E. Dormann (unpublished).
[59] E. Dormann, S. Matejcek, D. Saez de Jauregui, and A. Warth, J. Phys. IV **131**, 361 (2005).
[60] M. Glied, M. Drescher, and E. Dormann, J. Magn. Reson. **180**, 163 (2006).
[61] L. Forro, S. Bouffard, and L. Zuppirolli, J. Phys. (Paris), Colloq. **44**, C3-927 (1983).
[62] M. Sanquer, S. Bouffard, and L. Forro, Mol. Cryst. Liq. Cryst. **120**, 183 (1985).
[63] J. M. Delrieu, M. Beguin, and M. Sanquer, Synth. Met. **19**, 361 (1987).
[64] A. Georges, T. Giamarchi, and N. Sandler, Phys. Rev. B **61**, 16393 (2000).
[65] A. Schwartz, M. Dressel, G. Grüner, V. Vescoli, L. Degiorgi, and T. Giamarchi, Phys. Rev. B **58**, 1261 (1998).